IV International Conference on Computational Methods for Coupled Problems in Science and Engineering
COUPLED PROBLEMS 2011
M. Papadrakakis, E. Oñate and B. Schrefler (Eds)

COMPUTATIONAL FLUID-STRUCTURE INTERACTION SIMULATIONS FOR WIND INDUCED VIBRATIONS IN SILO GROUPS

J. HILLEWAERE*, J. DEGROOTE†, G. LOMBAERT*, J. VIERENDEELS† AND G. DEGRANDE*

*Department of Civil Engineering
Katholieke Universiteit Leuven
Kasteelpark Arenberg 40, B-3001 Heverlee, Belgium
e-mail: jeroen.hillewaere@bwk.kuleuven.be, bwk.kuleuven.be/bwm

†Department of Flow, Heat and Combustion Mechanics
Ghent University
St. Pietersnieuwstraat 41, B-9000 Gent, Belgium
e-mail: joris.degroote@ugent.be, www.ugent.be/ir/floheacom

Key words: Silo, Cylinder Group, Ovalling, Wind-Structure Interaction

Abstract. During a storm in October 2002, wind induced ovalling vibrations were observed on several empty silos of a closely spaced group consisting of 8 by 5 silos in the port of Antwerp (Belgium). First, a thorough understanding of the fluid flow around the group is required to clarify the underlying mechanisms for the vibration. Since the configuration and orientation of the group drastically change the pressure distribution on the silos of the group, the flow regime around and within the silo group has been simulated for 7 angles of incidence between 0° and 90°, leaving other parameters unchanged (e.g. spacing ratio, Reynolds number,...). The flow regime shows similarities with the flow within tube arrays (e.g. heat exchangers) and the flow around rectangular cylinders. By a 'one way coupling' of static (time averaged) and dynamic (fluctuating) pressure loadings on the cylinder surfaces, two probable causes of wind induced silo vibrations in the group are observed. The first, as a result of large static wind pressures and fluctuating drag and lift coefficients, might lead to rigid body motions of the statically deformed silos. The second, due to higher dynamic pressure oscillations, can excite ovalling oscillations in the third and fourth eigenmodes at the lee side of the group, corresponding with the lowest eigenfrequencies of the silos and the visually observed vibrations in 2002. Although it is shown by this 'one way coupling' that ovalling vibrations can be excited in the group, more advanced 'two way coupled' fluid-structure interaction simulations are required to determine the underlying mechanism inducing these aeroelastic deformations.

1 INTRODUCTION AND MOTIVATION

During a storm in October 2002, ovalling was observed on several empty silos near the corners of a group of 40 silos in the port of Antwerp (Belgium). No explanation for these wind induced instabilities or appropriate design guidelines to avoid them can be found in standards, e.g. Eurocode 1 [1]. A more realistic estimation of wind pressures and forces on the silos is required.

Numerical simulations are used to study the observed wind induced ovalling vibrations in the closely spaced Antwerp silo group, organized in 5 rows of 8 silos (figure 1). First, the specific structural behaviour with natural frequencies and according ovalling mode shapes of the silos is presented in the next section. In the third section, numerical simulation results of the turbulent wind flow, modelled as incompressible (low Mach number) flow, around the Antwerp silo group are shown. The influence of the angle of incidence α of the wind flow is investigated while other parameters such as spacing ratio, Reynolds number, etc. are left unchanged. For the present 8 by 5 closely spaced group configuration in a storm regime at post-critical Reynolds number ($\mathrm{Re} = 1.24\times10^7$), no experimental data are available. Therefore, validation of the numerical procedure is performed for the better documented case of 2D flow around a single cylinder in the post-critical regime. The more challenging simulations of the 2D flow around the entire silo group are furthermore validated qualitatively by assessing similarities of the present flow with the flow within tube arrays (e.g. heat exchangers) and the flow around rectangular cylinders. In the fourth section, the pressure distribution on the silos is investigated to verify whether and at which locations in the group pressure fluctuations can excite the ovalling eigenmodes of the silos. It is furthermore verified if this 'one way coupling' of structural and fluid dynamics model is sufficient to explain the existence of the ovalling vibrations in the silo group or whether more advanced 'two way coupled' fluid-structure interaction (FSI) simulations are required.

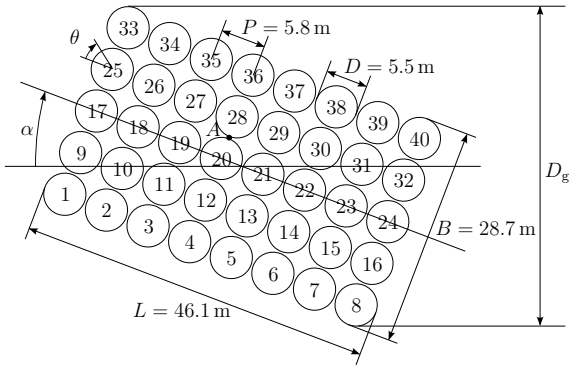

Figure 1: Plan view of the silo group with numbering of the invididual silos. Normative dimensions are given as well as definitions for the angle of incidence α and the angle θ on the circumference of an individual cylinder.

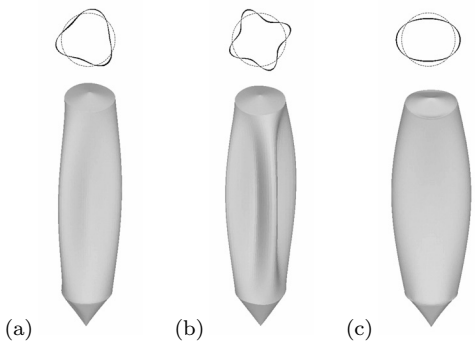

Figure 2: Selected ovalling eigenmodes of a single silo, (a) mode (1,3) at 3.93 Hz, (b) mode (1,4) also at 3.93 Hz and (c) mode (1,2) at 7.75 Hz [3].

2 STRUCTURAL BEHAVIOUR OF SILOS

Wind induced ovalling vibrations are an aeroelastic phenomenon where the cross section of the structure deforms as a shell without bending deformation with respect to the longitudinal axis of symmetry [2]. The ovalling mode shapes for the present thin walled empty silos have been studied by Dooms et al. [3] and are referred to by a couple (m, n) where m denotes the half wave number in the axial direction and n is the number of circumferential waves (figure 2). The lowest natural frequencies for these silos are found for ovalling mode shapes $(1, 3)$ and $(1, 4)$ at $f_\mathrm{n} = 3.93\,\mathrm{Hz}$.

3 AIR FLOW AROUND THE 8 BY 5 CYLINDER GROUP

The turbulent air flow around the 8 by 5 silo group is simulated numerically for 7 angles of incidence ($0° \leq \alpha \leq 90°$). Other influence parameters are left unchanged (e.g. spacing ratio, Reynolds number,...). After the introduction of the computational procedure, the case of a single cylinder in cross flow is calculated for validation. Similarities of the present flow around the silo group with the flow within tube arrays (e.g. heat exchangers) and the flow around rectangular cylinders are examined for qualitative validation of the simulation results. Hence, a distinction is implicitly made between vibrations related to the periodicity of the interstitial flow and vibrations caused by the large vortex structures behind the entire cylinder bundle.

3.1 Computational procedure

The 2D unsteady Reynolds averaged Navier-Stokes (URANS) discretized set of equations is solved in the Ansys FLUENT software package, using the hybrid shear-stress transport (SST) turbulence model. While 3D flow simulations over complex bodies have become possible in recent years, they remain very expensive and are therefore limited to moderate Reynolds numbers. On the contrary, 2D simulations are quite feasible, even for complex geometries and relatively high Reynolds numbers [4]. A coupled pressure-based calculation with a second order interpolation of the pressure, a second order upwind interpolation of momentum, turbulent kinetic energy k and specific dissipation rate ω is performed, while a second order implicit, unconditionally stable, time stepping method is used.

In the computations, the air density is $\rho = 1.25\,\mathrm{kg/m^3}$ and its dynamic viscosity is $\mu = 1.76 \times 10^{-5}\,\mathrm{Pa\,s}$. The boundaries of the rectangular computational domain are placed at distances of $9D$ to the central cylinder for the inlet and the lateral boundaries and $30D$ for the outlet of the domain, with D the diameter of the cylinder. Equivalently, $9D_\mathrm{g}$ and $30D_\mathrm{g}$ are used for the group configuration, with D_g the projected width of the silo group (figure 1). At the velocity inlet, an imposed free stream velocity $v_\mathrm{f} = 31.8\,\mathrm{m/s}$ is applied, based on Eurocode 1 for the present storm conditions in the vast and flat suburban surroundings of the silo group [1]. The outlet boundary is modelled as a pressure outlet with static pressure equal to the reference pressure. At the lateral boundaries symmetry

is imposed. The cylinder walls are considered smooth and no-slip boundary conditions are applied.

In these transient calculations, both grid and time step independency have been checked. The optimal mesh refinement is chosen and a time step of $\Delta t = 0.005\,\mathrm{s}$ is applied in the simulations.

3.2 Validation of single cylinder simulations

The Building Block Approach, introduced by the AIAA [5], allows for the validation of a proposed computational procedure with a simpler sub-system for which experimental data are available. The lack of experimental data for the 8 by 5 silo group makes this approach particularly appealing. The computational procedure is hence validated for the flow around a single cylinder.

For validation, the present numerical results are compared with experimental data and results of other (2D and 3D) numerical simulations. Several parameters are compared: the Strouhal number $\mathrm{St} = f_{\mathrm{vs}} L / v_{\mathrm{f}}$, the separation angle θ_{s} (figure 3) and the pressure coefficient, with f_{vs} the vortex shedding frequency, v_{f} the free stream velocity of the fluid and L the characteristic length, equal to the diameter D of the cylinder in the present case. The pressure coefficient along the circumference of a cylinder at a certain point in time is defined as

$$C_{\mathrm{p}}(\theta, t) = \frac{p(\theta, t) - p_{\mathrm{f}}}{\rho v_{\mathrm{f}}^2 / 2} \tag{1}$$

with p_{f} the free stream pressure. The time averaged pressure coefficient $\overline{C}_{\mathrm{p}}(\theta)$ is calculated as the average over multiple vortex shedding periods in time. The time averaged pressure coefficient for the present, single cylinder simulation is shown in figure 3 with $\theta_{\mathrm{s}} = 116°$ and $\mathrm{St} = 0.32$.

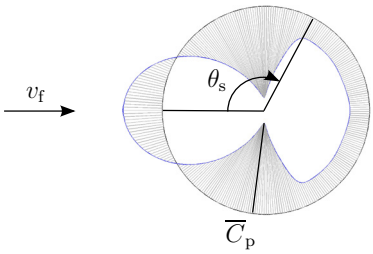

Figure 3: Time averaged pressure coefficient $\overline{C}_{\mathrm{p}}(\theta)$ on the circumference of the cylinder with indication of the free stream velocity v_{f} and the separation angle θ_{s}.

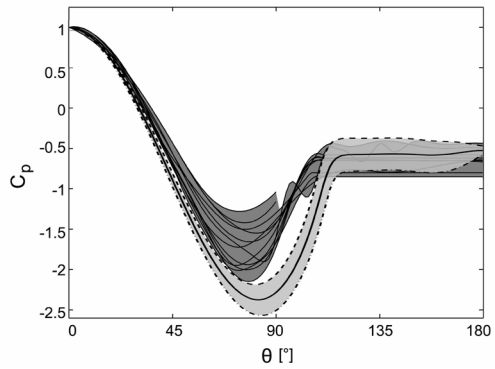

Figure 4: Measured pressure coefficients at Reynolds numbers from 0.73×10^7 to 3.65×10^7 [6] (dark grey zone) vs. present calculated maximal (dashed line), minimal (dash-dotted line) and time averaged pressure coefficients $\overline{C}_{\mathrm{p}}(\theta)$ (solid line) at $\mathrm{Re} = 1.24 \times 10^7$.

Zdravkovich [6] gives an elaborate overview of experimental pressure coefficients at Reynolds numbers from 0.73×10^7 to 3.65×10^7 (figure 4) where separation occurs between $\theta_s = 100°$ and 110°. For Reynolds numbers larger than 0.5×10^7, experimental smooth flow data of Zan [7] indicate that the Strouhal number remains at 0.2, whereas Schewe [8] found that it rises to about 0.3 as the Reynolds number approaches a value of 10^7; consistent with the tendency of the Strouhal number to rise from 0.2 to 0.3 in the range of Reynolds numbers between 10^6 and 10^7 [6].

Several numerical simulations have been reported in the literature for highly turbulent cross flows around circular cylinders. Younis et al. [9] performed 2D URANS simulations at $\mathrm{Re} = 0.35 \times 10^7$ with different turbulence models and report a Strouhal number of 0.28 and separation at $\theta_s = 120°$. Travin et al. [10] applied 3D DES for Reynolds numbers up to 3×10^6 and found Strouhal numbers 0.35 with separation at $\theta_s = 111°$.

The experimental and numerical data from literature show considerable scatter due to differences in Reynolds number, applied turbulence model, etc. However, generally good agreement is found between the present simulations ($\mathrm{St} = 0.32$, $\theta_s = 116°$) and the data from literature.

3.3 Discussion of the flow around the cylinder group

At the transverse corner cylinders of the group (e.g. cylinders 8 and 33 for $\alpha = 30°$, see figure 5c), shear layers in the outer flow are separated while approximately 10% of the flow is forced through the interstitial spaces in the group. These interstitial flows emerge at the lee side, join up and form several local recirculation zones in the wake that coalesce as they are carried downstream. One large scale vortex street is formed in the wake of the entire group, with a flow periodicity depicted by the Strouhal number St (table 1) with characteristic length $L = D_g$. For the smallest angles of incidence ($\alpha = 0°$ and 15°, figures 5a and 5b), it is clear that the emerging interstitial flows on the upper downstream side of the group (cylinders 33 to 40) are joined up and dragged downstream without forming local recirculation zones, due to the proximity of the separated shear layer. The same applies for the highest angles of incidence ($\alpha = 75°$ and 90°), where no such recirculation zones can be formed on the lower side of the group (cylinders 8 to 40).

The flow around the group as a whole resembles the behaviour of a single bluff body in cross flow, similarly to what Kareem et al. [11] observed for two closely spaced cylinders in tandem arrangement. Comparison with experimental data of the flow around a bluff rectangular cylinder in cross flow might hence be useful to assess the influence of porosity and rounded corners of the present 8 by 5 silo group. However, no experimental data can be found in literature for the present high Reynolds number. Knisely [12] performed experiments for a rectangular cylinder ($L/B = 1.67$) in cross flow, but at much lower Reynolds number ($1.2 \times 10^4 \leq \mathrm{Re} \leq 2.4 \times 10^4$). He found significantly lower Strouhal numbers (due to differences in Reynolds number and the rounded corners of the silo group), but also a sudden fall in Strouhal numbers for very small and very high angles of incidence ($\alpha \to 0°$ and $\alpha \to 90°$) when the separated shear layer reattaches to the

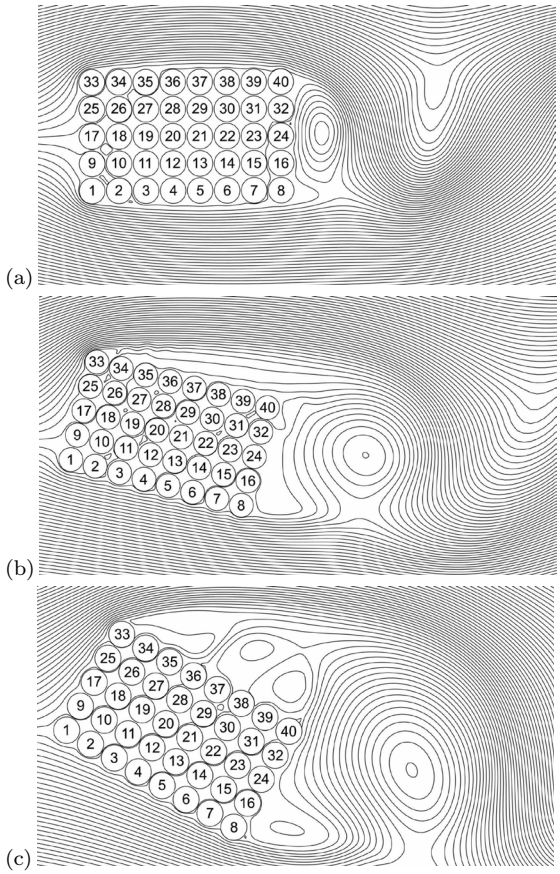

Figure 5: Velocity streamlines of the flow around the 8 by 5 cylinder group for an angle of incidence (a) $\alpha = 0°$ at $t = 80.0\,\text{s}$, (b) $\alpha = 15°$ at $t = 82.5\,\text{s}$, and (c) $\alpha = 30°$ at $t = 77.0\,\text{s}$.

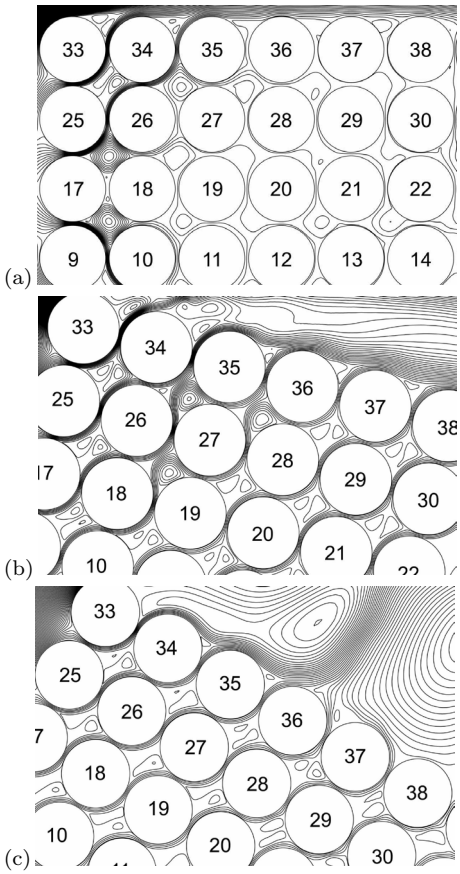

Figure 6: Detail of velocity streamlines for the interstitial space in the 8 by 5 cylinder group for an angle of incidence (a) $\alpha = 0°$ at $t = 78.5\,\text{s}$, (b) $\alpha = 15°$ at $t = 77.0\,\text{s}$, and (c) $\alpha = 30°$ at $t = 79.0\,\text{s}$.

cylinder surface. This sudden fall in Strouhal numbers cannot be observed in the present simulations: the emerging interstitial flows at the downstream side of the group prevent the shear layer from reattaching.

Table 1: Strouhal frequencies (f_{vs}) and Strouhal numbers (St) as a function of the angle of incidence (α) with respective projected width of the silo group (D_{g}).

α	[°]	0	15	30	45	60	75	90
D_{g}	[m]	28.7	38.4	45.9	50.6	52.3	50.7	46.1
f_{vs}	[Hz]	0.31	0.24	0.17	0.16	0.14	0.18	0.20
St		0.28	0.29	0.25	0.25	0.23	0.29	0.29

3.4 Discussion of the interstial flow in the cylinder group

Despite important differences (e.g. close spacing between cylinders and limitation to 40 cylinders), the interstitial flow pattern in the present simulations can be related to the flow through tube bundles that has been widely studied for the design of heat exchangers. Tube bundles are typically divided in two categories [13]: the in-line category where cylinders are arranged in square or rectangle arrays and the interstitial flow is mostly straight through the arrays, and the staggered category where cylinders are arranged in rotated square or triangle arrays and the flow is forced along wavy paths. The in-line, square configuration could apply to the cases with $\alpha = 0°$ and $\alpha = 90°$ for the cylinder group while for all other angles of incidence the staggered, rotated square arrangement would be applicable. As shown in figure 6, this is not always the case.

No straight flow pattern for $\alpha = 0°$ (figure 6a) and $\alpha = 90°$ is found. For in-line tube bundles, the presence of the subsequent row prevents the transitional eddies to form and roll-up and the eddies are carried away between the tubes by the jet-like interstitial flow [14]. The present cylinders, however, are too closely packed and these eddies are believed to partially or completely disappear in the distorted flow. Instead, the interstitial flow is not separated from the cylinder wall and follows a wavy path through the array, deflecting the flow up- and downward to the sides of the group, following the shortest path from the high pressures at the leading side of the group to the lower pressures at the lee side of the group. For other angles of incidence, interstitial flows resemble the wavy interstitial flow pattern of staggered tube bundles [13], e.g. for $\alpha = 30°$ (figure 6c). However, for $\alpha = 15°$ (figure 6b) and $\alpha = 60°$ (not shown), the regular wavy pattern is interrupted at arbitrary points in the array, where the interstitial flow separates from the cylinder surface and forms small recirculation zones or even results in local vortex shedding. These irregularities are probably related to the 2D character of the simulations and would not exist in 3D simulations where spanwise velocities are allowed [4].

4 Wind induced ovalling vibrations

Pressure distributions on the walls of the cylinders indicate whether wind induced vibrations of the silos can be excited. Distinction should be made between time averaged pressures on the one hand, which provide an indication of the static deflection of the silos and fluctuating pressures on the other hand, which represent the dynamic excitation of the silos. The silos on the transverse upstream corners of the group where the shear layer is separated (e.g. cylinders 1 and 33 for $\alpha = 0°$, figure 5a, or cylinders 8 and 33 for $\alpha = 30°$, figure 5c) are subject to the largest static pressures for all angles of incident flow. Combined with larger fluctuating drag and lift at these corners, this may result in observable rigid body motions of the statically deformed silos. This vibration phenomenon is however fundamentally different from the observed ovalling of the silos.

Ovalling vibrations can only be triggered by the fluctuating pressures on the cylinder

wall. Therefore, fluctuating pressure coefficients are determined as follows:

$$C'_{\mathrm{p}}(\theta, t) = C_{\mathrm{p}}(\theta, t) - \overline{C}_{\mathrm{p}}(\theta) \tag{2}$$

To investigate the contribution of these fluctuating pressures in the excitation of the eigenmodes of the silos, the pressure coefficients are harmonically decomposed into a series of cosine functions with circumferential wavenumber n, corresponding to the ovalling mode shapes of the axisymmetric structure (figure 2):

$$C'_{\mathrm{p}}(\theta, t) = \sum_{n=0}^{\infty} C'^{n}_{\mathrm{p}}(t)\cos(n\theta + \overline{\phi}_n) \tag{3}$$

Afterwards, the time history of the fluctuating pressure amplitudes $C'^{n}_{\mathrm{p}}(t)$ is transformed to the frequency domain by means of a FFT algorithm. Results for angle of incidence $\alpha = 30°$ and for circumferential wave numbers $n = 3$ and $n = 4$ are shown in figure 7 for cylinders 1, 8, 21, 33 and 40.

The frequency spectra for cylinders 1 and 33 (figures 7c and 7a) show no periodicities other than the low frequency contributions related to the large vortex shedding in the wake of the group. However, moving towards the lee side of the group, irregularities appear: higher frequencies also prevail in the frequency spectra for cylinders 8 and 40 (figures 7d and 7b). This frequency content at around 3 Hz to 4 Hz indicates that the third and fourth circumferential eigenmodes of the silos (both at eigenfrequencies of 3.93 Hz) will probably be excited. Moving downstream within the group, contributions at even higher frequencies are also encountered (e.g. cylinder 21, figure 7e). For other angles of incidence, these peaks in the frequency range between 3 Hz and 4 Hz are also found, confirming that the eigenmodes with the lowest eigenfrequencies, i.e. modes (1,3) and (1,4) (figure 2), will most likely be excited at the lee side of the silo group.

Hence, from the present 'one way coupling' of pressure fluctuations to the structural eigenmodes, it is found that ovalling vibrations may very well be excited at the lee side silos of the group. However, the underlying mechanism inducing these vibrations has not yet been determined.

It is generally accepted that there are three distinct mechanisms leading to vibrations in tube arrays [15, 16]. Firstly, forces can arise due to coincidence of a structural natural frequency with the vortex shedding frequency in the tube wake. Secondly, fluid-elastic instability (FEI) is based on self-excited forces which are caused by the interaction between tube motion and fluid flow [13]. Finally, turbulent buffeting forces arise due to turbulent fluctuations of the flow pressure. These forces arise as a response to flow turbulence, either initiated upstream or induced within the array itself [15].

Considering the large difference between the natural ovalling frequencies (figure 2) and the vortex shedding frequencies (f_{vs}, table 1), resonance effects can be excluded as a mechanism inducing ovalling vibrations in the silo group. Although periodicities in the interstitial flow may be very different from classical vortex shedding, these do not seem

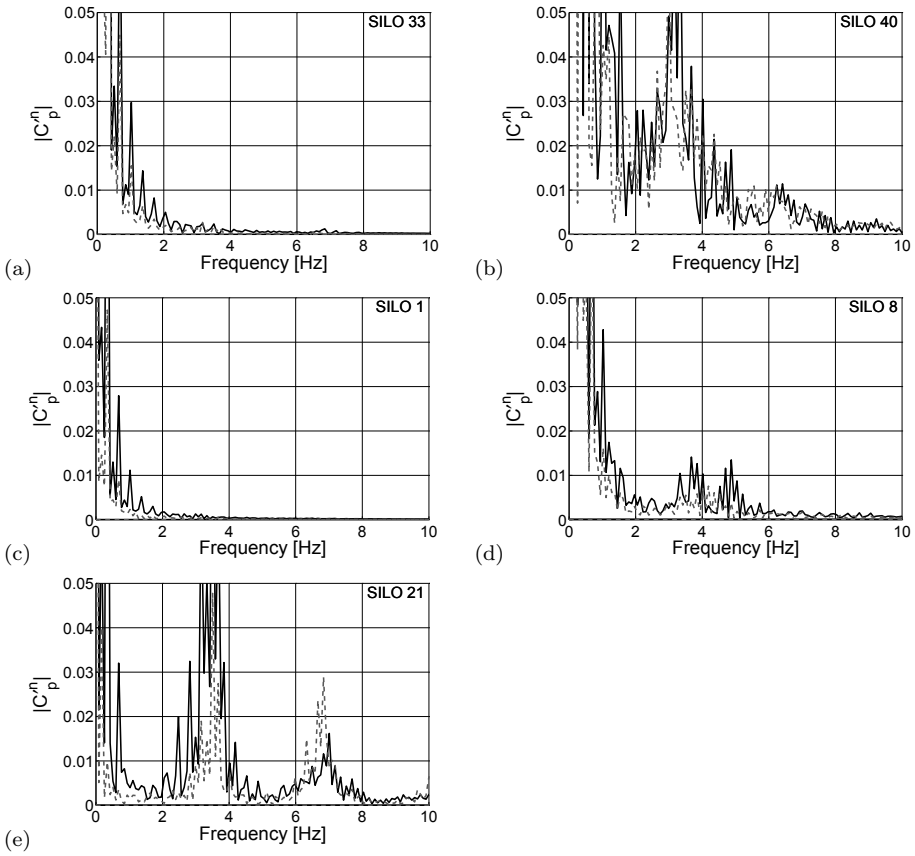

Figure 7: Frequency spectra for the amplitude of $C_{\mathrm{p}}^{\prime 3}$ (solid line) and $C_{\mathrm{p}}^{\prime 4}$ (dashed line) for angle of incidence $\alpha = 30°$ for (a) cylinder 33, (b) cylinder 40, (c) cylinder 1, (d) cylinder 8 and (e) cylinder 21.

to be related to ovalling, since they occur throughout the entire group whereas ovalling is only observed on the corner silos. Hence, FEI and/or turbulent buffeting are believed to be the primary causes of wind induced ovalling vibrations on the corners of the silo group.

Although it is confirmed by the present 'one way' coupling that ovalling vibrations may exist in the group arrangement, more advanced 'two way coupling' FSI calculations are required to verify the influence of FEI and turbulent buffeting. Since problems of aeroelasticity are typically considered weakly coupled problems, a partitioned coupling of the numerical structural model (e.g. finite element model of the silos) and the numerical fluid model (e.g. finite volume approach, considered here), with explicit coupling at the interface, could be applied. However, when modelling the incompressible flow around light and flexible structures, numerical instabilities as the artificial added mass effect may occur [17, 18]. The study of coupling schemes for wind-structure interaction problems is the topic of ongoing research.

5 CONCLUSIONS

In order to elucidate the occurence of ovalling oscillations on the empty corner silos of a 8 by 5 silo group in the port of Antwerp, the post-critical flow around this closely spaced cylinder group was simulated numerically. 2D URANS simulations for the entire group were performed for 7 angles of incidence α between 0° and 90°.

The group configuration and orientation of the group drastically change the flow regime, showing similarities with the fluid flow around bluff rectangular cylinders. The rounded corners and the porosity of the group have an important influence on the flow regime around the group. Approximately 10% of the incident flow penetrates the group and emerges at the lee side, preventing the shear layer from reattaching at very low and high angles of incidence ($\alpha \to 0°$ and $\alpha \to 90°$).

The flow in the interstitial spaces of the group is somewhat similar to the flow in tube bundles. Although the flow pattern is clearly different when the group is oriented parallel to the incident flow ($\alpha = 0°$ or $\alpha = 90°$), for an inclined orientation, the interstitial flow is very similar, following wavy paths through the array. For $\alpha = 15°$ and $\alpha = 60°$, at arbitrary locations in the array, irregularities are observed which are attributed to the 2D character of the numerical simulations.

To verify whether ovalling vibrations can be excited, the pressure distributions on the silos in the group are 'one way coupled' to the dynamic structural properties of the silos. Both static deflection (time averaged pressures) and dynamic excitation (fluctuating pressures) of the silos in the group configuration are considered. The silos near the transverse corners of the silo group, where the shear layer is separated, are subject to the largest static pressures for all angles of incident flow. However, to explain ovalling vibrations, dynamic fluctuating pressures have to be considered.

For all angles of incidence α, fluctuating pressures on the silos at the lee side of the group are seen to most likely excite the third and fourth structural ovalling eigenmodes, corresponding with the lowest natural frequencies of the silos. This observation corresponds with the visually detected ovalling eigenmodes with three and four circumferential wavelengths at the corner silos of the group during the 2002 storm in Antwerp.

The 'one way coupling' technique, presented here, is sufficient to explain the existence of the ovalling vibrations on the corner silos at the lee side of the silo group. Based on these simulations, the underlying physical mechanisms producing the flow periodicities and eventually inducing the ovalling vibrations are believed to be turbulent buffeting and/or FEI while resonance with some periodic vortex shedding frequency can be excluded. However, more advanced 'two way coupling' (FSI) simulations are required to verify the influence of FEI and turbulent buffeting.

ACKNOWLEDGEMENTS

The research in this paper has been performed within the frame of the FWO project G.0275.08 "Efficient analysis of fluid-structure interaction problems in structural dynam-

ics", funded by the Research Foundation Flanders (FWO Vlaanderen). The support of FWO is gratefully acknowledged.

REFERENCES

[1] BIN. *NBN EN 1991-1-4:2005 Eurocode 1: Actions on structures - Part 1-4: General actions - Wind actions*. Belgisch Instituut voor Normalisatie, (2005).

[2] Païdoussis, M.P., Price, S.J. and Suen, H.C. Ovalling oscillations of cantilevered and clamped-clamped cylindrical-shells in cross flow: An experimental-study. *Journal of Sound and Vibration*, (1982) **83**(4):533-553.

[3] Dooms, D., Degrande, G., De Roeck, G. and Reynders, E. Finite element modelling of a silo based on experimental modal analysis. *Engineering Structures*, **28**(4):532-542.

[4] Mittal, R. and Balachandar, S. Effect of three-dimensionality on the lift and drag of nominally two-dimensional cylinders. *Physics of Fluids*, (1995) **7**(8):1841-1865.

[5] Versteeg, H.K. and Malalasekara, W. *An Introduction to Computational Fluid Mechanics: The Finite Volume Method*. Pearson Education Limited, Essex, England, second edition (2007).

[6] Zdravkovich, M.M. *Flow Around Circular Cylinders, Volume 1: Fundamentals*. Oxford University Press, Oxford, England, (1997).

[7] Zan, S.J. Experiments on circular cylinders in crossflow at Reynolds numbers up to 7 million. *Journal of Wind Engineering and Industrial Aerodynamics*, (2008) **96**(6-7):880-886.

[8] Schewe, G. On the force-fluctuations acting on a circular-cylinder in cross-flow from subcritical up to transcritical Reynolds-numbers. *Journal of Fluid Mechanics*, (1983) **133**(AUG):265-285.

[9] Younis, B.A. and Przulj, V.P. Computation of turbulent vortex shedding. *Computational Mechanics*, (2006) **37**(5):408-425.

[10] Travin, A., Shur, M., Strelets, M. and Spalart, P. Detached-eddy simulations past a circular cylinder. *Flow, Turbulence and Combustion*, (2000) **63**(1-4):293-313.

[11] Kareem, A., Kijewski, T. and Lu, P.C. Investigation of interference effects for a group of finite cylinders. *Journal of Wind Engineering and Industrial Aerodynamics*, (1998) **77-78**:503-520.

[12] Knisely, C.W. Strouhal numbers of rectangular cylinders at incidence: a review and new data. *Journal of Fluids and Structures*, (1990) **4**(4):371-393.

[13] Zdravkovich, M.M. *Flow Around Circular Cylinders, Volume 2: Applications*. Oxford University Press, Oxford, England, (2003).

[14] Hunt, J.C.R. and Eames, I. The disappearance of laminar and turbulent wakes in complex flows. *Journal of Fluid Mechanics*, (2002) **457**:111-132.

[15] Price, S.J., Païdoussis, M.P., Macdonald, R. and Mark, B. The flow-induced vibration of a single flexible cylinder in a rotated square array of rigid cylinders with a pitch-to-diameter ratio of 2.12. *Journal of Fluids and Structures*, (1987) **1**(3):359-378.

[16] Weaver, D.S., Lian, H.Y., and Huang, X.Y. Vortex shedding in rotated square arrays. *Journal of Fluids and Structures*, (1993) **7**(2):107-121.

[17] Causin, P., Gerbeau, J.F. and Nobile, F. Added-mass effect in the design of partitioned algorithms for fluid-structure problems. *Computer Methods in Applied Mechanics and Engineering*, (2005) **194**(42-44):4506-4527.

[18] Förster, C., Wall, W.A. and Ramm, E. Artificial added mass instabilities in sequential staggered coupling of nonlinear structures and incompressible viscous flows. *Computer Methods in Applied Mechanics and Engineering*, (2007) **196**(7):1278-1293.